Contents

Chapter 1

Search for neutral MSSM Higgs Bosons in $A/h/H \to \tau^+\tau^- \to e\mu + 4\nu$ decays

In light of the recent discovery of a Higgs boson with mass of ~ 126 GeV at LHC [16, 17], it remains an open question whether this new particle is the only missing piece of the electroweak symmetry breaking sector or whether it is one of several Higgs bosons predicted in some theories that go beyond the SM. The most recent measurements [125–128] of its properties shows this new boson to be, within experimental uncertainties, fully compatible with the SM Higgs boson. Nevertheles, such a new particle can also still be accommodated within several theories beyond the standard model (BSM), among all of them, Supersymmetry is a theoretically favoured scenario as the most predictive framework beyond the Standard Model.

This chapter presents the search for the neutral MSSM Higgs bosons decaying into pairs of tau leptons in the fully leptonic final state, published in Ref. [][1] as a part of the search for the neutral MSSM Higgs bosons in all final states of the tau leptons decay. The search is based on 20.3 fb^{-1} of 8 TeV data recorded by the ATLAS experiment during 2012 at the Large Hadron Collider. The chapter is organized as follows: a brief summary of the MSSM Higgs sector and an introduction to the analysis strategy is given in Section 1.1, while the event selection and categorization are described in Section 1.2. In Section 1.3 the estimation of the background is described and in Section **??** methods to evaluate sys-

[1] to Sandra: I'll remove this sentence if Conf note wont be ready in time

tematic uncertainties are discussed. Finally, in section **??**, an overview of the statistical methods employed along with the corresponding result of the search are presented.

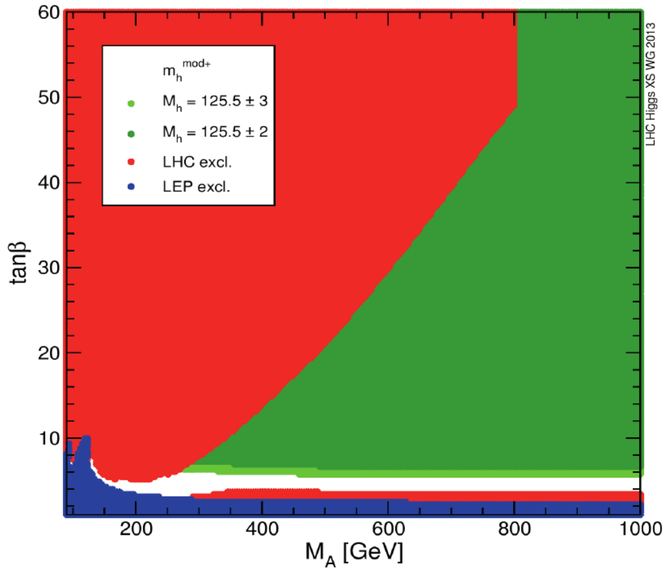

Figure 1.1: Excluded and allowed regions of the $m_A - \tan\beta$ parameter space for the m_h^{mod+} MSSM benchmark scenario. Excluded regions are determined based on direct Higgs boson searches at LEP (blue) and LHC (red). The two green bands correspond to the parameter regions which are compatible with the assumption that the lightest MSSM Higgs boson, h, has a mass respectively of $M_h = 125.5 \pm 2$ (dark green) or 125.5 ± 3 GeV (light green). For more detail see [4].

1.1 Introduction

1.1.1 The Higgs Sector in the MSSM

In the Minimal Supersymmetric extension of the Standard Model (MSSM) [36, 37] the Higgs sector is composed of two Higgs doublets of opposite hyper-charge, resulting in five observable Higgs bosons: two of these are neutral and CP-even (h,H), one is neutral and CP-odd (A) and two are charged ($H^{\pm}$). At tree level their properties such as masses, widths and branching ratios can be predicted in terms of only two parameters, often chosen to be the mass of the CP-odd Higgs boson m_A and the ratio of the vacuum expectation values of the two Higgs doublets $\tan\beta$ (for more details see chapter **??**). The MSSM predicts the existence of a Higgs boson with properties that resemble those of a SM Higgs boson in large regions of its parameter space. This is usually the case for the lightest Higgs boson, h, while the other two, H and A, tend to be degenerate in mass and decouple from gauge bosons. On the other hand, the couplings of the latter two Higgs bosons with down (up) type fermions are enhanced (suppressed) proportionally to the value of $\tan\beta$, meaning that for large $\tan\beta$ bottom-quark and τ lepton will play an important role for the Higgs bosons production and its decays.

The two most relevant MSSM Higgs bosons production mechanisms at the LHC are gluon fusion, $gg \to A/H/h$, and the production in association with b-quarks, $pp \to b(b)A/h/H$, the latter becoming increasingly important for large values of

$\tan\beta$. These two are the only production mechanisms considered in this analysis. Assuming there are no decays into supersymmetric particles since these are too heavy, the favored neutral MSSM Higgs bosons decay mode is the decay into a pair of b-quark and antiquark, $A/h/H \to b\bar{b}$. This is followed, for the CP-odd A and CP-even H Higgs bosons, by the decay into pairs of τ leptons. Given that it is very difficult to distinguish the former decay from the large $b\bar{b}$ background, the decay mode $A/h/H \to \tau^+\tau^-$ provides the highest sensitivity in the search for neutral MSSM Higgs bosons.

Searches for neutral MSSM Higgs bosons have been performed at LEP [64], the Tevatron [65] and the LHC [66,67]. In the following the search for the neutral MSSM Higgs bosons in the final state $A/h/H \to \tau^+\tau^- \to e\mu + 4\nu$ is presented. This search is complementary to the searches in other $\tau^+\tau^-$ final states characterized by the presence of one or two hadronicaly decaying τ leptons. Despite of the fact that the $\tau\tau$ branching ration in $e\mu + 4\nu$ is only 6%, this decay channel provides a sensitivity to the signal comparable to those in other $\tau\tau$ final states, especially for low m_A values. This is mainly due to the high transverse momentum treshold at the trigger level for hadronicaly decaying τ leptons.

As it is impractical for an experimental search to explore the full parameter space of the MSSM, which has many free paramers, several benchmark scenarios are introduced by fixing all except m_A and $\tan\beta$ parameters to values typical for most interesting physics cases. With the recent Higgs boson discovery, benchmark scenarios of the MSSM have been updated to accommodate for new experimental constraints. As an example, Figure 1.1 shows the currently excluded and allowed regions of the MSSM parameter space for the m_h^{mod+} updated benchmark scenario. In this scenario a large region of the $m_A - \tan\beta$ parameter space is compatible with the assumption that the observed Higgs boson correspond to the supersymmetric SM-like Higgs boson, h. A large part of this parameter space is still experimentally unexplored, this is a strong motivation to pursue the search for additional neutral MSSM Higgs bosons.

1.1.2 Signal and Background Processes

Signal events in which the neutral MSSM Higgs bosons decay through $A/h/H \to \tau^+\tau^- \to e\mu + 4\nu$ process are characterized by the presence of one electron and one muon of opposite charge. These two leptons are isolated and have relatively high transverse momenta. In addition, four neutrinos contribute to the missing transverse energy in the event. Figure 1.2 shows leading order Feynman diagram for the two considered signal production modes, gluon fusion and in association with b-quarks. The presence (absence) of a b-jet in the final state serves as a main caracteristic for the event categorization in the latter (former) case, as described later on.

The described signal topology is common to several other known SM background processes which in general have higher cross sections than the sought signal. The dominant background processes are the $Z/\gamma^* \to \tau^+\tau^-$ production either via Drell-Yan process or in association with jets and the top quark production ($t\bar{t}$ and single top quark production). Additional significant background contributions originate

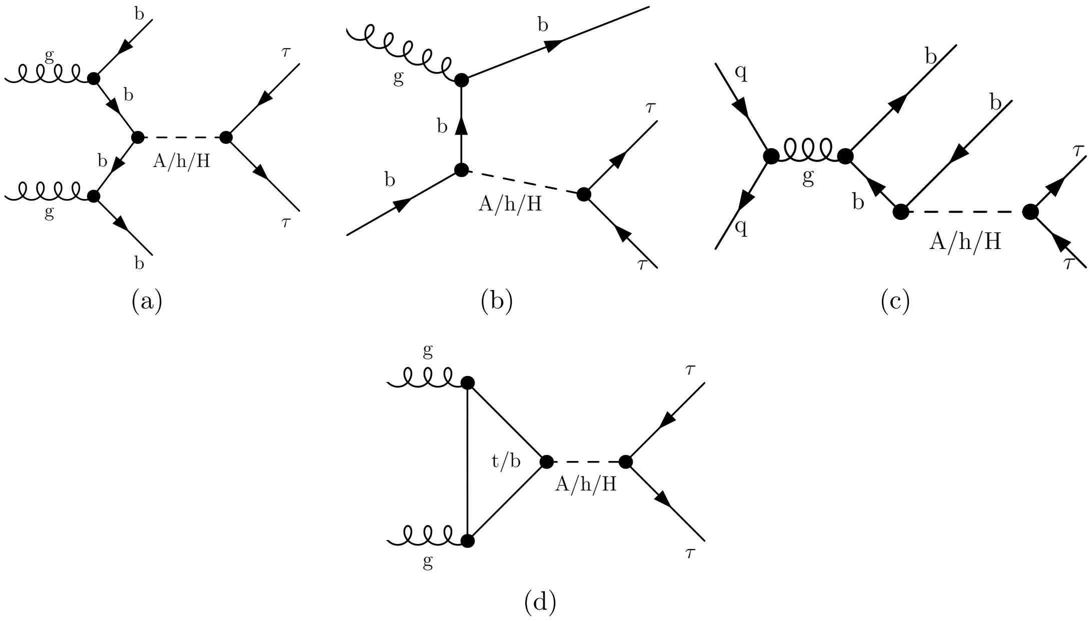

Figure 1.2: Feynman diagram for the production of the neutral MSSM Higgs bosons in association with b-quarks (a,b,c) and via gluon fusion (d) process, subsequent decay in tau lepton pairs is considered.

from the dibosons production (WW, WZ, ZZ) and QCD multi-jet events with non-prompt leptons from hadron decay. Vector boson production ($W \to \ell\nu$ or $Z \to \ell\ell$, where $\ell \equiv e, \mu$) in association with jets is also considered, but has small impact on the total background contamination. Examples of leading order Feynman diagrams for the dominant background processes are shown in Figure 1.3. The production cross sections times the relevant branching fraction for signal and background processes are summarized in Table 1.1.

1.1.3 Analysis Strategy

In this thesis a search for the MSSM $A/h/H \to \tau^+\tau^- \to e\mu{+}4\nu$ decays is presented. The $ee + 4\nu$ and $\mu\mu + 4nu$ final states are not considered since a large background background contribution is expected from $Z \to ee$ and $Z \to \mu\mu$ decays, respectively, such that the sensitivity of the search in these final state is significantly reduced.

Candidate events are selected based on the topological properties of the Higgs boson production and decay. The presence of exactly one electron and one muon is required in each event. Electron and muon are required to be isolated and of opposite electrical charge. The events are categorized into two mutually orthogonal event categories.In the so called *b-vetoed* category, the absence of any b-tagged jets is required, thus searching mainly the signal produced via gluon fusion. The main background process in this category is $Z/\gamma^* \to \tau\tau$. In contrast, the presence of exactly one b-tagged jet is required in the so called *b-tagged* event category, searching predominantly signal produced in association with b-quarks. The requirement of a b-jet in the final state suppresses the $Z/\gamma^* \to \tau\tau$ background. Consequently, $t\bar{t}$ and

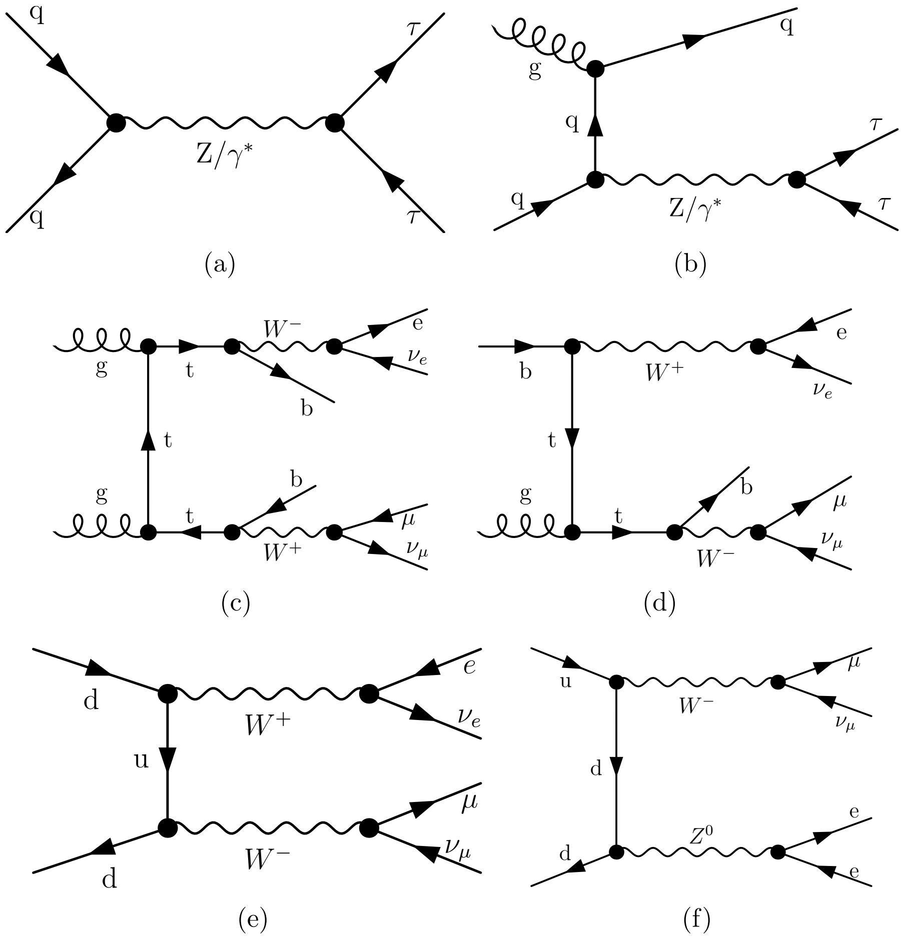

Figure 1.3: Examples of tree level Feynman diagrams for the production and decays of the most relevat backgrounds. The production of $Z/\gamma^* \to \tau^+\tau^-$ either via Drell-Yan process or in association with jets is shown in (a) and (b), top quark pair and single top quark production in (c) and (d), while examples of WW and WZ production are shown in (e) and (f) respectively.

Process	Cross-section (pb) [× BR]
Signal ($m_A = 150$ GeV, $\tan\beta = 20$, m_h^{mod} scenario)	
$gg \to A/h/H \to \tau\tau \to e\mu + 4\nu$	0.24/0.20/0.95
$pp \to b\bar{b}A/h/H \to \tau\tau \to e\mu + 4\nu$	0.53/0.05/0.49
Backgrounds	
$W \to \ell\nu$+jets	12.22×10^3
$Z/\gamma^* \to \ell\ell$+jets	5.5×10^3
$t\bar{t} \to \ell\ell + X$	137.3
Single top quark ($t-$, $s-$ and $Wt-$channels) $\to \ell + X$	28.4, 1.8, 22.4
Dibosons (WW, WZ and ZZ) $\to \ell\ell + X$	20.6, 6.8, 1.55

Table 1.1: The cross sections multiplied by the relevant branching ratios (BR) for signal and the considered background processes. The symbol ℓ stands for $\ell = (e, \mu, \tau)$. Signal cross sections are calculated for the m_h^{mod} scenario assuming $m_A = 150$ GeV and $\tan\beta = 20$. The masses of the other two neutral MSSM Higgs bosons are in this case $m_H = 151$ GeV and $m_h = 125$ GeV.

single top quark production are the main background processes in this category. Further selection criteria are introduced in both categories, these are optimized to enhance the signal produced by the corresponding production mode.

The search is performed within the MSSM m_h^{mod} benchmark scenario scanning the $m_A - \tan\beta$ plane in the ranges $90 \leq m_A \leq 300$ GeV and $5 < \tan\beta < 60$. The prediction of the signal event yields and kinematical distributions are evaluated by simulation. The contribution of the dominant $Z/\gamma^* \to \tau\tau$ background process is measured in a dedicated signal-depleted control data sample, in order to reduce the systematic uncertainties of the simulation. Similarly, the QCD multi-jet background contribution is also estimated from dedicated data control sample since it represent a challenge for simulated events. Contribution of all other background processes is estimated from simulation. The modeling of the background processes is validated using different signal-depleted validation data samples and good agreement is found.

The systematic uncertainties on cross section calculations and the modeling of the detector response taken into account for simulated signal and background processes. For background processes that are measured with data, the uncertainties of the corresponding measurement methods are evaluated.

The final statistical interpretation of the data is based on the comparison of the observed $\tau\tau$ invariant mass distributions with the prediction of the background-only and signal-plus-background hypotesis. Exclusion limits on the signal production are set by means of a binned profiled likelihood ratio test statistic. The limits are interpreted within the MSSM m_h^{mod} scenario in terms of the constraints on the m_A and $\tan\beta$ values. Furthermore, the results are also expressed in a less model-dependent way in terms of the upper limits on the cross section for the production of a generic Higgs boson ϕ with a mass m_ϕ via the production processes $pp \to b\bar{b}\phi$ and $gg \to \phi$.

1.1.4 Data and Simulated Event Samples

Data Sample

The presented result are based on proton-proton collision data collected at the LHC during 2012 at a center-of-mass energy of $\sqrt{s} = 8$ TeV, corresponding to an integrated luminosity of 20.3 fb^{-1}. The events used in this analysis are recorded using a combination of a single electron and combined electron-muon triggers. Only recorded events in which all relevant components of the ATLAS detector were fully operational are considered. Additional data quality requirements are applied to each event according to [113]. These requirements assure the rejection of events with jet activity in known noisy calorimeter regions.

Signal Samples

Signal production via the gluon fusion process, $gg \to A/H/h$, was simulated with POWHEG [77] and the associated $b\bar{b}A/H/h$ production with SHERPA [78]. The pseudo-scalar Higgs boson samples were generated in the mass range from 90 GeV to 300 GeV assiuming $\tan\beta = 20$, all three neutral Higgs bosons $(A/h/H)$ are assumed to decay with the same kinematic properties. Appropriate re-weighting of the production cross sections is applied to simulate other $\tan\beta$ values. The m_h^{mod} MSSM benchmark scenario is assumed.

Background Samples

The production of W and Z/γ^* bosons in association with jets was simulated with the ALPGEN [70] generator. The $t\bar{t}$ process was generated using the POWHEG generator. The single top quark production via s-channel and in Wt process were generated using MC@NLO [72], while single top quark production via t-channel was generated with the AcerMC [73] generator. Diboson processes (WW, WZ, ZZ) were generated with the HERWIG [74] generator. For all ALPGEN and MC@NLO event samples described above, the parton shower and hadronisation were simulated with HERWIG and the underlying event activity with the JIMMY [75] programme. Different sets of parton density functions (PDFs) are used depending on the generator: CTEQ6L1 [79] is used by ALPGEN and AcerMC while CT10 [80] is used by SHERPA, POWHEG and MC@NLO.

TAUOLA [82] and PHOTOS [83] are used to model the tau lepton decay and additional photon radiation from charged leptons in the leading-log approximation, respectively.

The ATLAS detector response is simulated for all generated samples using the GEANT4 [84, 85] package, the reconstruction of physics objects, described in chapter **??**, is performed with the same software used also for the data. The effects of the simultaneous recording of additional proton collisions from the same or neighboring bunch crossings (pile-up) are taken into account in the simulation.

1.2 Event Selection and Categorization

1.2.1 The Common Selection Criteria

According to the characteristic properties of signal events, each event in data and simulation should satisfy the selection criteria described in the following. Since these are shared by both the b-tagged and b-vetoed event category, they are referred to as common selection criteria:

(i) A trigger selection, requiring the presence of a single electron with $p_T > 24$ GeV, or alternativaley, an electron with $p_T > 12$ GeV togheter with a muon with $p_T > 8$ GeV.

(ii) At least one reconstructed vertex with more that three associated tracks. This selection is aimed to reject background from cosmic muons.

(iii) Exactly one reconstructed "Tight" electron with $|\eta| < 1.37$ or $1.52 < |\eta| < 2.47$. The electron should have $p_T > 15$ or 25 GeV depending on the trigger that selected the event.

(iv) Exactly one "Combined" muon with $|\eta| < 2.5$ and $p_T > 10$ GeV.

(v) The electron should be isolated with $E_T^{cone}/p_T < 0.08$ and $P_T^{cone}/p_T < 0.06$.

(vi) The muon should be isolated with $E_T^{cone}/p_T < 0.04$ and $P_T^{cone}/p_T < 0.06$.

(vii) Muon and electron should be of opposite charge.

(viii) Overlap removal between electron, muon, τ_h and jets is performed.

(ix) The event is rejected if at least one hadronic τ lepton decay is found with the transverse momentum of the corresponding τ-jet $p_T > 15$ GeV.

(x) To reduce QCD-multijet background contamination, the invariant mass obtained from the sum of the electron and muon four-momenta should be greather than 30 GeV.

Details on the definition of physics objects and the applied quality criteria can be found in chapter **??**.

Events accepted by the common selection criteria are categorized into the *b-tagged* and *b-vetoed* event categories by requiring the presence of exactly one b-tagged jet or the absence of any b-tagged jet in the event, respectively. A jet is considered b-tagged if it has $p_T > 20$ GeV, $|\eta| < 2.5$, JVF > 0.5 and it passes the selection of the $MV1$ b-tagging algorithm at 70% of efficiency for b-quark, $\epsilon_b^{t\bar{t}}$. Further selection criteria are applied to each category and optimized separately, as described in the following.

Category	Selection
b-vetoed	No b-tagged jets $\Delta\phi(e-\mu) > 1.6$ $\sum \cos\Delta\phi > -0.4$
b-tagged	Exactly one b-tagged jet $\Delta\phi(e-\mu) > 2$ $\sum \cos\Delta\phi > -0.2$ $H_T < 100$ GeV $P_{T\mu} + P_{Te} + E_T^{miss} < 100$ GeV

Table 1.2: Summary of the event selection criteria in the b-tagged and b-vetoed event categories, applied after the common event selection has been performed.

1.2.2 b-vetoed Event Category

A veto on the presence of b-tagged jets in the final state allows for the selection of signal events which are produced predominantly via gluon fusion. In this event category the $Z/\gamma^* \to \tau\tau$ process is an irreducible background due to the same topology of the Higgs and Z boson decay. Other background processes can still be discriminated against the signal due to their kinamatic properties. The τ leptons from the Higgs boson decay are higly boosted and so are their decay products, this results in significantly different lepton kinematic with respect to diboson or $t\bar{t}$ background processes. Firstly, the electron and muon from Higgs boson decay will be more likely emitted back-to-back. This is illustrated in Figure 1.4(a), showing the angular distance between the two leptons in the transverse plane $\Delta\phi_{e,\mu} = |\phi_e - \phi_\mu|$ for the signal and relevant background processes. Secondly, the neutrinos from the Higgs boson decay will be more likely collinear with the charged leptons, thus, the angular correlation between the direction of the missing transverse energy and the two leptons, derived as:

$$\hat{E}_T^{miss} \cdot (\hat{P}_T^{\mu} + \hat{P}_T^{e}) = cos(\Delta\phi_{E_T,\mu}) + cos(\Delta\phi_{E_T,e}) = \sum_{\ell} cos(\Delta\phi_{E_T,\ell})$$

is expected to tend to zero, as is shown in Figure 1.4(b). These two features can be used to discriminate the signal from the W boson, top quark or in dibosons background processes. No further selection criteria are applied in this event category, as it has been shown that no significant improvement of the analysis sensitivity can be achieved. The exact selection criteria are listed in Table 1.2, while in Table 1.3 the predicted number of background and signal events after each stage of selection are reported.

1.2.3 b-tagged Event Category

The request of exactly one b-tagged jet in the b-tagged event category selects predominantly signal events produced in b-quarks associated production mode. Background processes with b-jet activity, as the top quark and single top quark production become enhanced compared to the $Z/\gamma^* \to \tau\tau$ background. Also in this category selection requirement on $\Delta\phi(e-\mu)$ and $\sum\cos\Delta\phi$ are imposed as described for the b-vetoed event category, in order to reduce the top quark and diboson background contributions. Further selection criteria specific for this category are employed as described below.

Given the relatively low jet activity of the signal events, it is possible to discriminate these from top quark production. The top quark proces are very likely to have two or more highly enegetic jets in the event, unlike the signal b-jet which are relatively low energetic. Weak jet activity is ensured by requesting the sum of the jets transverse momenta, H_T, in the event to be small. The H_T distribution is shown in Figure 1.4(c). The jets used for the calculation of the H_T value should have $p_T > 30$ GeV, $|\eta| < 4.5$ and JVF > 0.5 (if $|\eta| < 2.5$).

Another feature that discriminate top quark pair production from the Higgs boson signal is the higher invariant mass of the former final state, as the highest Higgs mass considered for the presented search is 300 GeV. The sum of electron and muon transverse momenta with E_T^{miss} is used as a corresponding discriminating variable, whose distribiution is shown in Figure 1.4(d) .

The summary of the exact optimized selection criteria for the b-tagged event category is shown in Table 1.2. In Table 1.4 the predicted number of background and signal events after each stage of selection in the b-tagged event category is reported.

1.2.4 Mass Reconstruction with MMC Technique

Acurate invariant mass reconstruction of a di-τ resonace is a challenging task due to the undetected neutrinos. In the presented analysis a total of four neutrinos are involved in the final state, two for each of the τ lepton decays. The invariant mass depends on eight uknowns given by the two sums of neutrino four-momenta, one for each τ lepton decay. These unknowns can be constrained by four parameters obtained from the measured missing transverse energy and from the τ lepton mass, using the following equations:

$$\begin{aligned} \vec{E}_T^{miss} &= \vec{P}_T^{mis_1} + \vec{P}_T^{mis_2} \\ M_{\tau_i}^2 &= m_{mis_i}^2 + m_{vis_i}^2 + 2\mathbf{P}_{vis_i} \cdot \mathbf{P}_{mis_i} \end{aligned} \tag{1.1}$$

where the index i runs over the two τ leptons in the event. $\vec{P}_T^{mis_i}$, m_{mis_i} and $\mathbf{P}_{mis_i}$ are respectively the transverse momentum, the invariant mass and the four momentum of the pair of neutrinos originating from the decay of the i-th τ lepton with mass M_τ. The subscript *vis* indicates instead quantities related to the charged lepton from the corresponding τ lepton decay. The remaining four degrees of freedom can be further constrained, for example, assuming that the neutrinos are collinear to the electron or muon from the corresponding τ lepton decay. Those approximation, however, introduces limitations on the mass resolution.

In this analysis, the so-called "Missing Mass Calculator" (MMC) algorithm is used to calculate the most likely invariant mass of the di-τ system for a given event topology. The implementation of the MMC method in this search is based on [129].

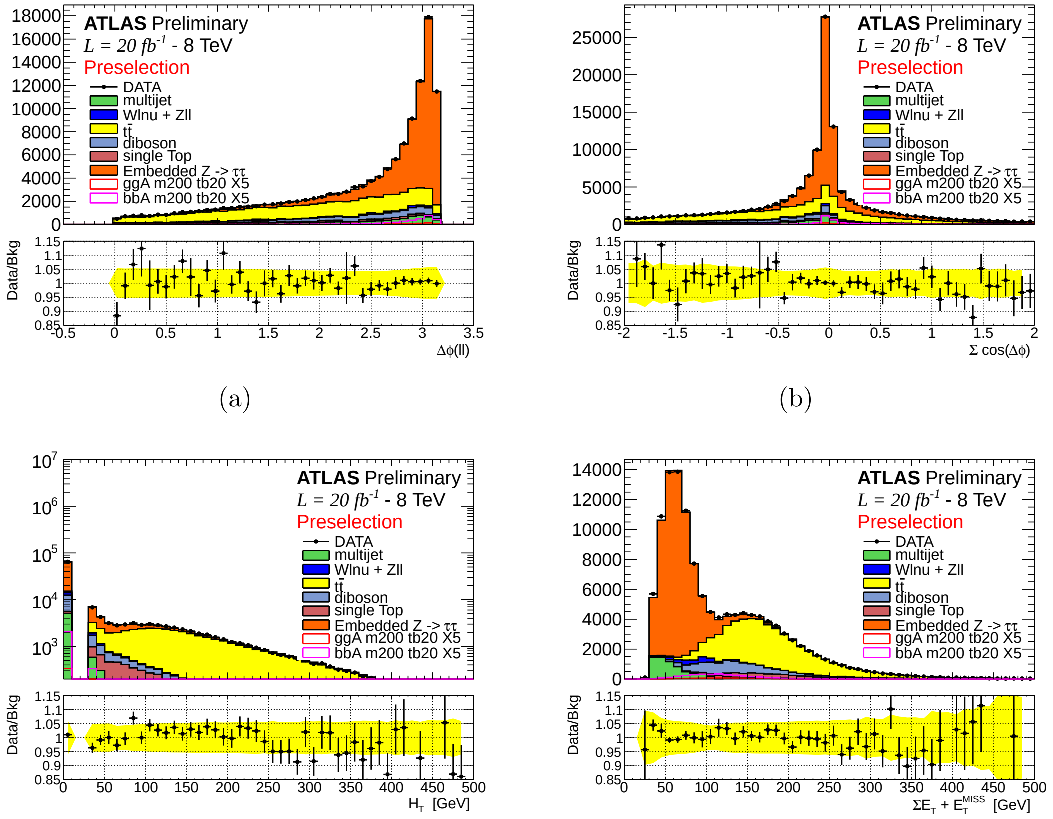

(a) (b) (c) (d)

Figure 1.4: Distributions of relevant discriminating variables shown after the common selection has been applied. The prediction of the background model is compared to data. The contribution of the $Z/\gamma^* \to \tau\tau$ and QCD multi-jet background processes is measured in dedicated signal-depleted control data samples, the prediction for all the other bakground processes is obtained from simulation. The yellow band represents the total systematic uncertainty for the background model prediction (see Section ??).

	Common Selections	n(b-jet)=0	$\Delta\phi(e-\mu) > 1.6$	$\sum \cos\Delta\phi > -0.4$
Data	125886	89155	-	- -
Multi-jet	6693 $\pm$ 456	6357 $\pm$ 461	5322 $\pm$ 438	4137 $\pm$ 339
$Z \to \ell\ell$	569 $\pm$ 48	564 $\pm$ 48	516 $\pm$ 47	434 $\pm$ 44
$W \to \ell\nu$	1625 $\pm$ 155	1604 $\pm$ 155	1145 $\pm$ 125	714 $\pm$ 101
Dibosons	9338 $\pm$ 48	9235 $\pm$ 48	7358 $\pm$ 43	4002 $\pm$ 31
$t\bar{t}$	40632 $\pm$ 106	7707 $\pm$ 46	5044 $\pm$ 37	3416 $\pm$ 31
Single Top	4449 $\pm$ 44	1664 $\pm$ 27	1124 $\pm$ 22	682 $\pm$ 18
$Z/\gamma^* \to \tau\tau$	61503 $\pm$ 68	60440 $\pm$ 67	58078 $\pm$ 65	55303 $\pm$ 64
Signal			-	-

Table 1.3: Number of observed and predicted signal and background events, after each selection stage in the b-vetoed event category.

	n(b-jet)=1	$\Delta\phi$	$\sum \cos\Delta\phi$	$P_{T\mu} + P_{Te} + E_T^{miss}$	H_T
Data	23352	-	-	-	-
Multi-jet 330 ± 40	208 ± 27	135 ± 22	114 ± 17	100 ± 15	
$Z \to \ell\ell$	5.2 ± 1.8	2.3 ± 1.1	2.3 ± 1.1	1.7 ± 1.0	0.9 ± 0.8
$W \to \ell\nu$	20 ± 6	15 ± 6	13 ± 6	10 ± 6	10 ± 6
Dibosons	99 ± 5	63 ± 4	36.4 ± 3.0	14.8 ± 1.8	13.3 ± 1.8
$t\bar{t}$	19810 ± 70	9680 ± 50	6450 ± 50	808 ± 15	350 ± 10
Single Top	2456 ± 33	1223 ± 23	784 ± 18	122 ± 7	99 ± 7
$Z/\gamma^* \to \tau\tau$	952 ± 9	625 ± 7	540 ± 7	482 ± 6	421 ± 6
Signal		-	-	-	-

Table 1.4: Number of observed and predicted signal and background events, after each selection stage in the b-tagged event category.

The MMC algorithm solves the equations 1.1 for a set of points in a grid of a four-dimensional parameter space. The four independent variables are chosen to be $m^2_{mis_i}$ and $cos\theta^*_i$, the latter defined as the angle between the charged lepton from the τ lepton decay and the boost direction of the τ lepton. The di-τ invariant mass in each event is then calculated for each given point of the parameter space. Each solution is weighted by the probability that a τ lepton decay assumes a given configuration. The probability of a given configuration is predicted by means of simulation using PYTHIA generator supplemented with TAUOLA package. The invariant mass of the di-τ system, $m^{MMC}_{\tau\tau}$, is then defined as the maximum of the weighted invariant mass distribution obtained from all scanned points.

The resolution of the missing transverse energy measurement impacts the resolution of the invariant mass obtained with the $m^{MMC}_{\tau\tau}$ method. To improve the E_T^{miss} resolution, a scan over a six-dimensional parameter space is performed in a similar manner as described above. For this purpose, the value of $\vec{E}_T^{miss}$ is also considered unknown and a scan is performed over all possible values constrained by the measured E_T^{miss} and its corresponding uncertainty.

Figure 1.5 shows the $m^{MMC}_{\tau\tau}$ invariant mass distribution after after the common selection and after applying the full selection in both event categories.

1.3 Background Prediction and Validation

This section describes the strategies for the prediction of the background contributions and validation of these predictions. Monte Carlo simulation is extensively used to model the kinematic properties of the background and signal processes. However, since the simulation of any process is usually prone to systematic uncertainties due to a non-perfect description of the pileup effects, underlying event and detector performance, the background contributions from $Z/\gamma^* \to \tau\tau$ and QCD multi-jet process are estimated using dedicated signal-free control data samples, as described respectively in section 1.3.3 and 1.3.2. Contributions of other background processes, such as $t\bar{t}$, single top quark, dibosons, $Z \to ll$ + jets (where $l = e, \mu$) and W + jets, are estimated from simulation. Given the relatively large $t\bar{t}$ background contribution, a dedicated study to validate this background prediction has been made as described in section 1.3.1.

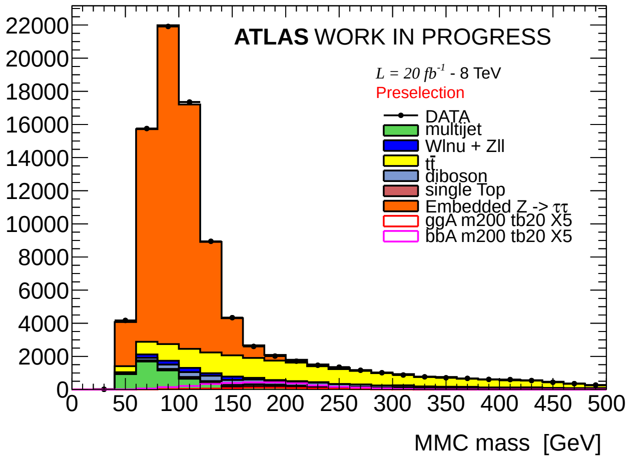

(a)

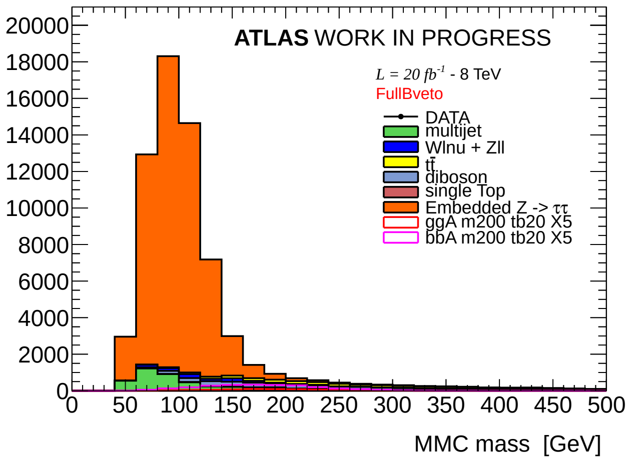

(b)

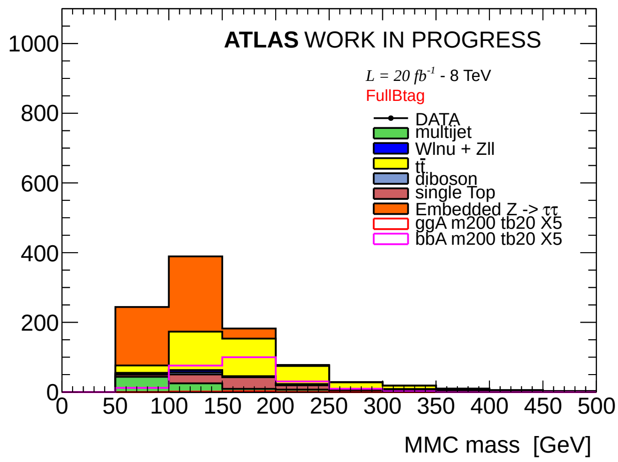

(c)

Figure 1.5: Observed and expected distribution of the invariant di-τ mass $m_{\tau\tau}^{MMC}$ for different stage of analysis selections.

Data Sample	Relative Lepton Charge	Lepton Isolation
A (signal sample)	OS	isolated
B	SS	isolated
C	OS	anti-isolated
D	SS	anti-isolated

Table 1.5: Control data samples for the measurement of the QCD multi-jet background contribution. The samples are defined by the requirements on the relative charge sign of the two leptons (OS,SS) and the isolation criteria applied on them (isolated or anti-isolated). See text.

A good agreement between data and background prediction is found after the common selection, as can be seen in Figure 1.4 and Figure 1.6.

1.3.1 Validation of the $t\bar{t}$ Background Prediction

The background contribution from top quark pair production is estimated using a sample of simulated events generated with POWHEG-PYTHIA Monte Carlo generator. Since this is one of the major background processes for the presented analysis a careful validation of the predicted contribution is needed. For this purpose signal-depleted data validation sample enriched with $t\bar{t}$ events by requiring the presence of exactly two b-tagged jets in all the events passing the common selection. Figures 1.7 and 1.8 show the distributions for a set of kinematic properties and all discriminating variables obtained with this data sample. Good agreement between data and Monte Carlo prediction is found with overall ratio of the observed to the predicted number of $t\bar{t}$ events of $0.998 \pm 0.011(\text{stat.}) \pm 0.110(\text{sys.})$. The total systematic uncertainty on the ratio is dominated by the uncertainty of the b-tagging efficiency.

1.3.2 Multi-jet Background Measurement

The QCD multi-jet process represents an important background, especially in the b-vetoed event category, due to its high cross-section and the relatively low threshold on the lepton p_T used in this analysis. The contribution of this background is evaluated by the so-called ABCD data-driven technique. The ABCD method splits the sample of data events after the common selection into four sub-samples: the signal sample (A), defined by the event selections criteria described in Section 1.2 and three signal-depleted control data sample (B,C,D), which are orthogonal to each other and are enriched in multi-jets events. The three control data samples are defined by inverting the requirements on the relative sign of the electron and muon charge and on the isolation criteria. Both the calorimetric and tracking isolation criteria described in Section 1.2.1 are inverted for each electron and muon with respect to the nominal values, thus defining the so-called anti-isolated leptons. The data are divided into four samples of events with leptons of opposite sign charge (OS) or same sign charge (SS) with respectively isolated or anti-isolated leptons, as summarized in Table 1.5.

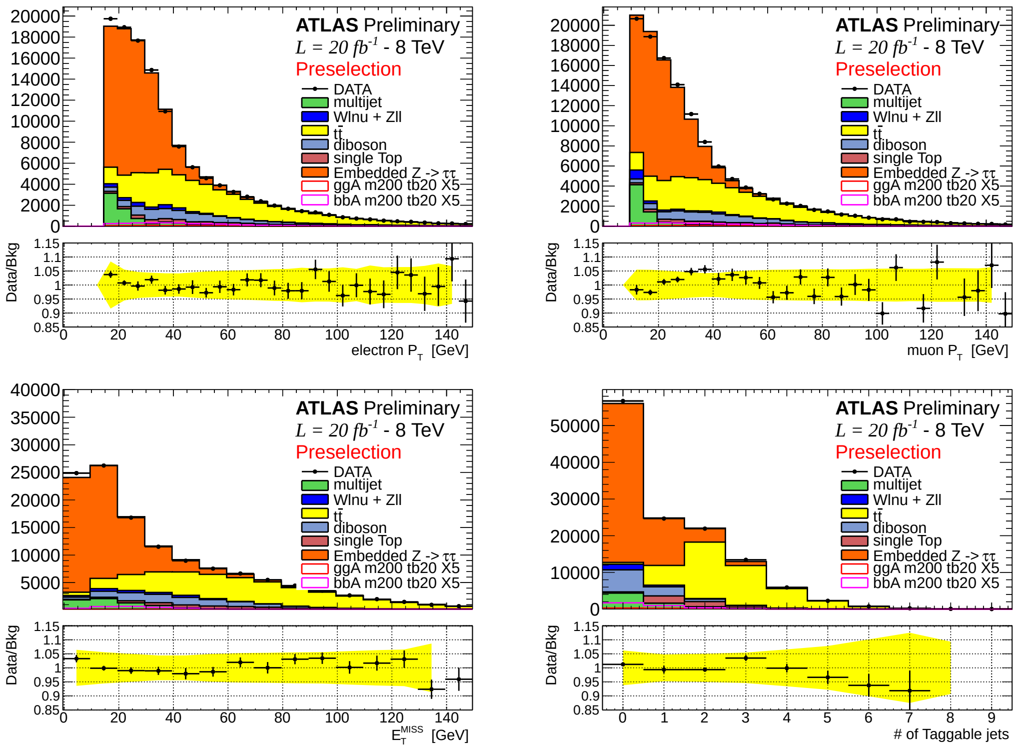

Figure 1.6: Observed and expected distribution of kinematic variables after common selections. The prediction of the background model is compared to data. The contribution of the $Z/\gamma^* \to \tau\tau$ and QCD multi-jet background processes is measured in dedicated signal-depleted control data samples, the prediction for all the other bakground processes is obtained from simulation. The yellow band represents the total systematic uncertainty for the background model prediction.

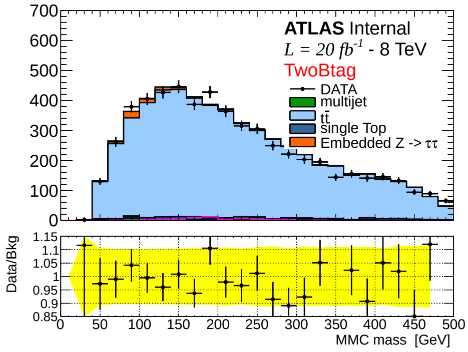

(a)

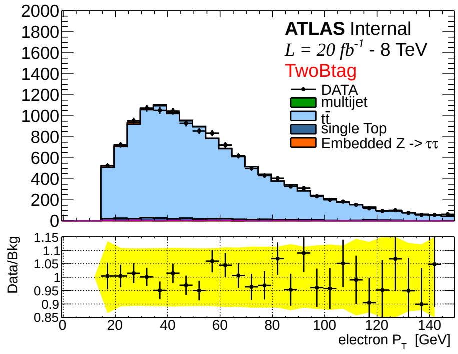

(b)

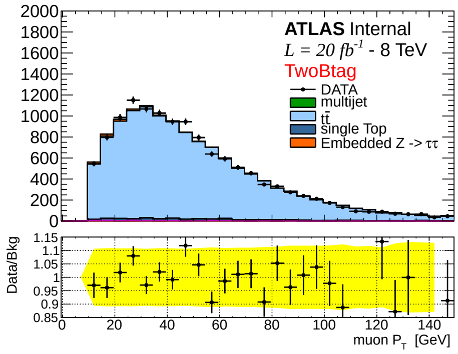

(c)

Figure 1.7: Observed and expected distributions of a) the di-τ invariant mass $m_{\tau\tau}^{MMC}$, b) the electron transverse momentum $p_T(e)$ and c) the muon transverse momentum $p_T(\mu)$ in the $t\bar{t}$ validation sample. The error bars on the observed to the predicted events ratio indicates the statistical uncertainty, whereas the yellow band indicates the total systematic uncertainty of this ratio.

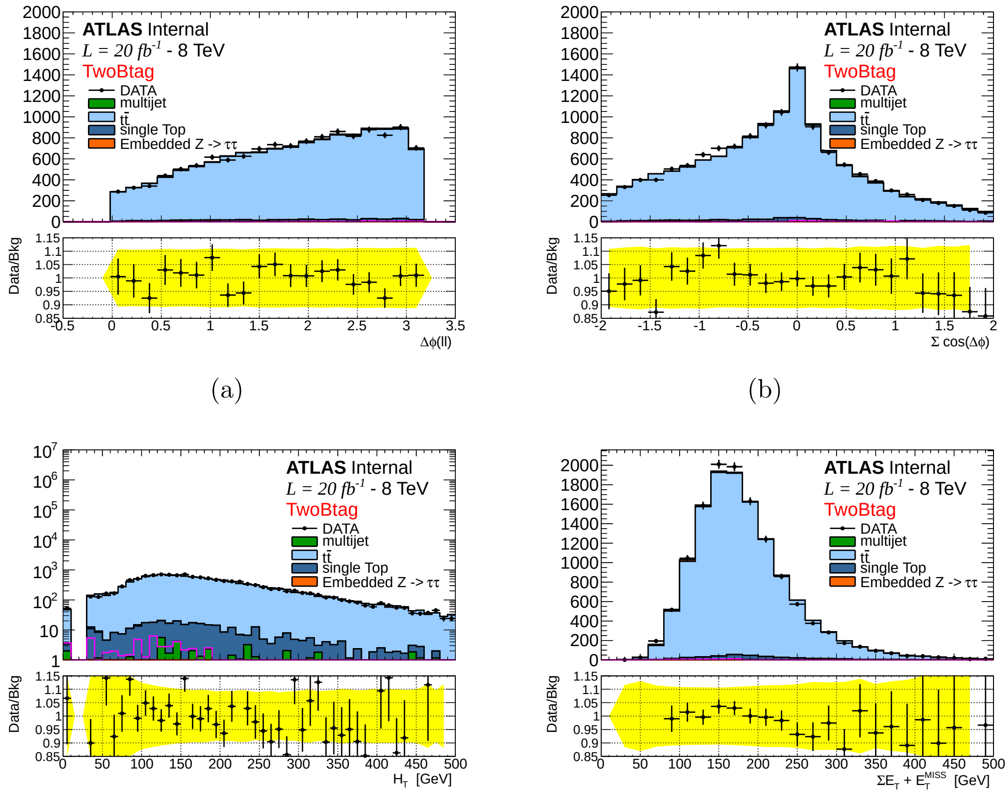

(a) (b) (c) (d)

Figure 1.8: Observed and expected distributions of the discriminating variables, (a) $\Delta\phi(e-\mu)$, (b) $\sum\cos\Delta\phi$, (c) $p_{T\mu}+p_{Te}+E_T^{miss}$ and (d) H_T in the $t\bar{t}$ validation sample. The error bars on the observed to the predicted events ratio indicates the statistical uncertainty, whereas the yellow band indicates the total systematic uncertainty of this ratio.

The ABCD method assumes that there is no correlation between the relative charge and lepton isolation in QCD multi-jet events, or in other words that the ratio of OS/SS events is uncorrelated with the lepton isolation criteria. In this case, the number (N_A) of QCD multi-jet events in the signal sample A can be estimated from the yields (N_B, N_C, N_D) of multi-jet events in the control samples B, C and D, using the equation

$$N_A = N_B \times \frac{N_C}{N_D} = N_B \times R_{QCD} \tag{1.2}$$

To obtain the pure QCD multi-jet event yields in the data control samples, the contribution from contaminating electroweak (W+jets, Z+jets and dibosons) and top quark processes ($t\bar{t}$, single top quark production) is subtracted in each control sample based on the prediction from simulation. Tables 1.7 and 1.6 show the observed event yield in each control sample at different stages of the event selection along with the predictions of non-QCD background contributions which are subtracted. Signal contamination has been evaluated in all three control samples for different signal mass points. For the range of m_A and tanβ values considered in this analysis, the highest signal contamination is seen in sample B for the mass point $m_A = 300$ GeV and tan$\beta = 50$, where a contamination of 0.2% is observed[2].

The modeling of the shapes of kinematic distributions in QCD multi-jet events is given by the data sample B. The events in this sample are expected to have similar kinematic properties as in the signal sample. A drawback of this choice is a rather low number of events and a higher contamination with non-QCD process compared to samples C and D. Sample B is chosen to avoid a shape bias due to isolation requirements at the trigger level, since the single-electron trigger allready imposes isolation requirements. Figure 1.9 shows the comparison of the electron p_T distributions in sample B and D. In the latter sample high-p_T electrons are suppressed as they do not pass the trigger selection. Eventually the trigger isolation requirement could also bias the ratio R_{QCD}. This possibility has been carefully studied in a dedicated study as reported in Appendix **??**. To a good approximation, the mentioned trigger effects cancel out in the ratio R_{QCD} and no additional systematic uncertainty needs to be taken into account.

To test the predictions of the ABCD method an additional validation sample has been defined with the following selection criteria after applying the common selection:

- $E_T^{miss} < 20$ GeV
- $H_T < 70$ GeV and $p_{T\mu} + p_{Te} + E_T^{miss} < 50$ GeV
- $0 < m_{\tau\tau}^{MMC} < 80$ GeV

This validation sample is designed to enhance the multi-jet background contribution with respect to $Z/\gamma^* \to \tau\tau$ keeping the final state kinematics as similar as possible to the signal sample. Figure 1.10 shows the $m_{\tau\tau}^{MMC}$ distribution for this validation sample with and without the b-tagging requirements. Agreement between data and the background predictions is found within statistical and detector-related systematics uncertainty.

Systematic uncertainties are assigned on the scaling factor R_{QCD} and on the shape of the discriminating variable $m_{\tau\tau}^{MMC}$ to take into account any correlation between the isolation and the relative charge of the leptons as detailed in Section **??**.

1.3.3 $Z \to \tau\tau$ + Jets Background Measurement

The $Z/\gamma^* \to \tau\tau$ decays are the major source of background to the presented analysis, calling for its thorough understanding. Unfortunately, for a light Higgs boson, it is impossible to fully discriminate the $Z/\gamma^* \to \tau\tau$ decays from the signal and thus a dedicated signal-free data control sample cannot be defined. However, thanks to the small Higgs boson coupling to muons, $Z \to \mu\mu$ decays provide a good starting point to model $Z/\gamma^* \to \tau\tau$ events based on data. A hybrid approach relying on data and simulation known as the "embedding" is used for this purpose. The $Z \to \mu\mu$ event

[2] This contamination signal originates mainly from the production in association wit b-quarks and, as it scales with the cross section, it will be an order of magnitude smaller for $\tan\beta = 20$.

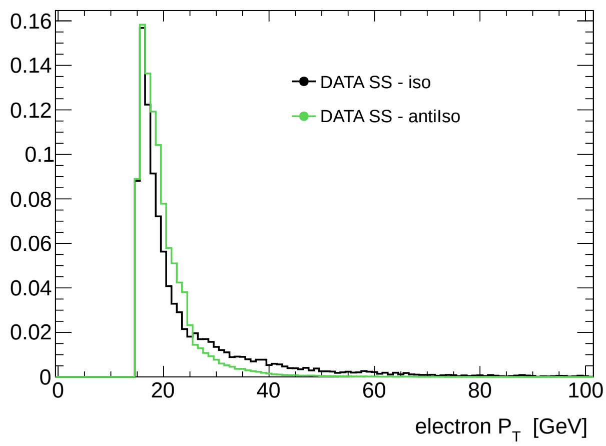

Figure 1.9: Comparison of the electron p_T distribution in control samples B and sample D, showing the bias due to the trigger. The histograms are normalized to the same area.

Event Selection		B	C	D	R_{QCD}
Common Selection	Data	6189	604628	312901	1.929 $\pm$ 0.004
	non-QCD	2510 $\pm$ 180	1090 $\pm$ 30	730 $\pm$ 35	
B-veto	Data	5673	558217	284847	1.960 $\pm$ 0.004
	non-QCD	2220 $\pm$ 180	710 $\pm$ 30	415 $\pm$ 30	
$\Delta\phi(e-\mu)$	Data	4610	532583	271404	1.962 $\pm$ 0.005
	non-QCD	1700 $\pm$170	580 $\pm$ 30	345 $\pm$ 30	
$\sum\cos\Delta\phi$	Data	3417	486747	247712	1.965 $\pm$ 0.005
	non-QCD	1120 $\pm$ 100	370 $\pm$ 20	230 $\pm$ 20	
$m_{\tau\tau}^{MMC} > 0.$	Data	3177	479967	244276	1.965 $\pm$ 0.005
	non-QCD	1000 $\pm$ 100	300 $\pm$ 17	190 $\pm$ 20	

Table 1.6: Number of observed events and the predicted non-QCD contribution at different stages of the event selections for b-veto category. The error on the R_{QCD} ratio is of statistical nature only.

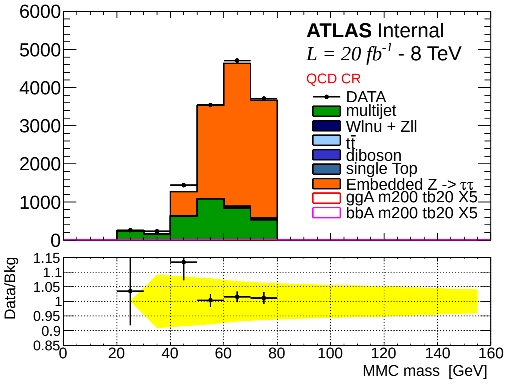

(a)

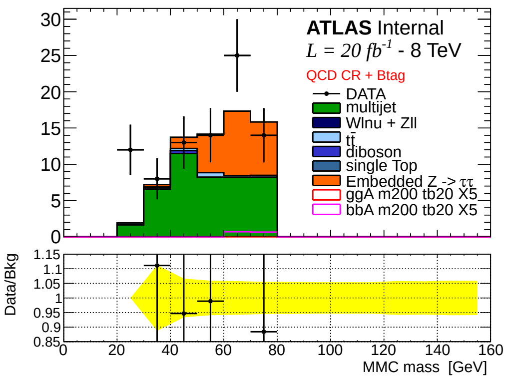

(b)

Figure 1.10: $m_{\tau\tau}^{MMC}$ distribution obtained with QCD validation samples defined in Section 1.3.2, without (a) and with an additional requirement of exactly one b-tagged jet in the final state (b).

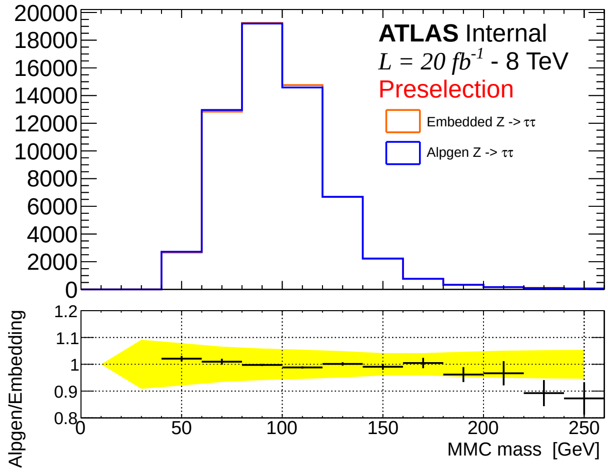

Figure 1.11: Comparison of the $m_{\tau\tau}^{MMC}$ distributions obtained from the ALPGEN $Z/\gamma^* \to \tau\tau$ simulation and from the embedding technique after the requirements of th common selection has been applied. The yellow bad indicates the total systematic uncertainty relative to the ALPGEN simulation sample.

candidates are selected in data. The two muons from the Z decay are then substituted with the decay products from simulated τ lepton decays. The energy deposit in the calorimeter and the reconstructed tracks in a cone of given size around the muon are subtracted and substituted with the corresponding predictions from the τ lepton decay. These τ leptons have the same kinematic properties as the original muons. Further details on the embedding technique may be found in [86, 87].

As the Trigger is not simulated in the described embedded samples, only the shapes of kinematic distributions are modelled by the embedded sample, while the $Z \to \tau\tau$ event yield is normalized to ALPGEN $Z/\gamma^* \to \tau\tau$ prediction at a common selection stage. Furthermore, a set of corrections as described in [88], is applied to unfold from the original $Z \to \mu\mu$ trigger and reconstruction efficiency. Subsequently, the trigger and reconstruction efficiency the $e\mu + 4\nu$ final state are emulated by means of event weights.

The embedding technique has been validated in several studies detailed in [86, 88], demostrating a reliable performance of the embedding technique and a good description of data. In the context of this analysis, Figures 1.11 and 1.12 show comparisons of various kinematic distributions between data, embedded and ALPGEN $Z/\gamma^* \to \tau\tau$ events at the common selection stage. No significant differences are seen between for the $m_{\tau\tau}^{MMC}$ distribution. Other relevant discriminating variables, such as the E_T^{miss} and the number of b-jets in the final state, are slightly better described by the embedded $Z/\gamma^* \to \tau\tau$ sample, as expected due to the imperfect modeling of these variables with simulation.

The embedded sample is based on the selected $Z \to \mu\mu$ event candidates in data. The $Z \to \mu\mu$ selection criteria assure a rather pure $Z \to \mu\mu$ sample. However, further event selection criteria used in the presented analysis, for example the b-tagging requirements, could enhance the contamination of this sample with events

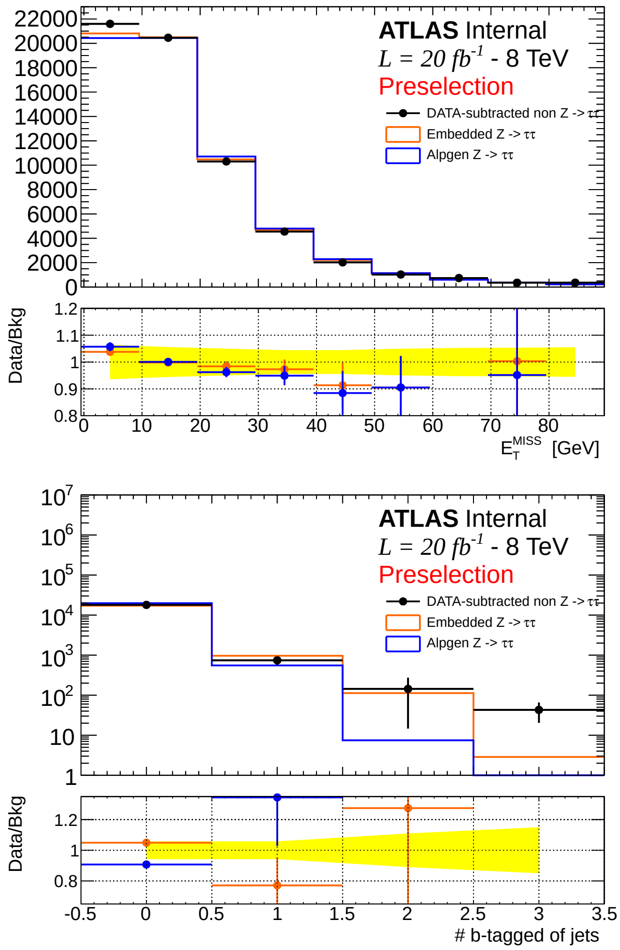

Figure 1.12: Comparison of the (a) E_T^{miss} and (b) b-tagged jet multiplicity distributions in embedded and ALPGEN $Z/\gamma^* \to \tau\tau$ events after the requirements of the common selection has been applied. Data are superimposed after subtracting the contribution of non-$Z/\gamma^* \to \tau\tau$ processes.The yellow bad indicates the total systematic uncertainty relative to the ALPGEN simulation sample.

from other processes. Dedicated studies have been made to estimate the $t\bar{t}$ and QCD multi-jet contamination in the embedded sample. The $t\bar{t}$ contamination is estimated by evaluating the yield of embedded $Z \to \tau\tau$ events in a validation sample with two b-tagged jets (as described in Section 1.3.1). These events are assumed to originate solely from the $t\bar{t}$ process and the corresponding yield in the signal sample is extrapolated from simulation. Table 1.8 summarizes the evaluated top quark contamination in the embedded $Z \to \tau\tau$ sample, separately for the two event categories. The multi-jet contamination can be estimated starting from the yield of embedded events in the sample C defined by the ABCD method. It is assumed that all events in this validation sample are QCD multi-jet events. The QCD multi-jet contamination of the embedded events in the signal sample can be estimated as:

$$N_A^{QCD-emb} = N_C^{QCD-emb} \times \frac{N_B^{\mu\mu}}{N_D^{\mu\mu}} = N_B \times R_{QCD}^{\mu\mu} \tag{1.3}$$

The transfer factor $R_{QCD}^{\mu\mu}$, is evaluated using a di-muon final state with same kinematic selection criteria as for $Z \to \mu\mu$ candidates entering the embedding procedure. Table 1.9 shows the estimated contamination of QCD multi-jet in the embedded sample. Contamination effects are considered negligible.

Event Selection		B	C	D	R_{QCD}
Common Selection	Data	6189	604628	312901	1.929 ± 0.004
	non-QCD	2510 ± 180	1090 ± 30	730 ± 35	
B-tag	Data	419	44619	27257	1.64 ± 0.01
	non-QCD	215 ± 10	310 ± 12	277 ± 13	
$\Delta\phi(e-\mu)$	Data	230	38810	23316	1.67 ± 0.01
	non-QCD	104 ± 6	200 ± 10	175 ± 7	
$\sum \cos\Delta\phi$	Data	149	31379	18779	1.67 ± 0.02
	non-QCD	67 ± 5	127 ± 8	114 ± 6	
$\sum H_T$	Data	83	27781	15626	1.78 ± 0.02
	non-QCD	23 ± 4	25 ± 3	22 ± 3	
$p_{T\mu} + p_{Te} + E_T^{miss}$	Data	71	27735	15590	1.78 ± 0.02
	non-QCD	10 ± 3	22 ± 3	18 ± 2	
$m_{\tau\tau}^{MMC} > 0.$	Data	70	27634	15522	1.78 ± 0.02
	non-QCD	9 ± 3	20 ± 3	17 ± 2	

Table 1.7: Number of observed events and the predicted non-QCD contribution at different stages of the event selections for b-tag category. The error on the R_{QCD} ratio is of statistical nature only.

	Yield of embedded events	Transfer factor	Estimated events in signal sample	Contamination
b-tag	84 ± 9	$(2.6 \pm 0.1) \times 10^{-2}$	2.2 ± 0.2	0.5 %
b-veto	84 ± 9	$(1.74 \pm 0.02) \times 10^{-1}$	15 ± 2	0.03 %

Table 1.8: Evaluation of the $t\bar{t}$ contamination in the embedded $Z \to \tau\tau$ sample using a two b-tag validation sample. The transfer factor is a multiplicative factor obtained from simulation that allows to extrapolate the measuremet from the validation sample into the signal sample.

	Yield of embedded events in QCD control sample C	Transfer factor	Estimated events in signal sample	Contamination
B-tag	12 ± 3	$(7 \pm 1) \times 10^{-3}$	$(8.4 \pm 0.3) \times 10^{-2}$	0.03 %
B-veto	390 ± 20	$(2.5 \pm 0.1) \times 10^{-2}$	10.0 ± 0.5	0.02 %

Table 1.9: Evaluation of the QCD multi-jet contamination in the embedded $Z \to \tau\tau$ sample using the control sample with OS anti-isolated events (sample C). The transfer factor $R_{QCD}^{\mu\mu}$ is the multiplicative factor that allows to extrapolate the measured events in control sample C into the signal sample. The transfer factor is evaluated using di-muon events with same kinematic properties as the $Z \to \mu\mu$ candidates entering the embedding procedure.

Bibliography

[1] G. Altarelli, *"Collider Physics within the Standard Model: a Primer,"* arXiv:1303.2842 .

[2] S. P. Martin, *"A Supersymmetry primer,"* In *Kane, G.L. (ed.): Perspectives on supersymmetry II* 1-153 [hep-ph/9709356].

[3] A. Djouadi, *The Anatomy of Electroweak Symmetry Breaking Tome II: The Higgs Bosons in the Minimal Supersymmetric Model*, Phys. Rep. 459 (2008) 1.

[4] S. Heinemeyer *et al.* [LHC Higgs Cross Section Working Group Collaboration], "Handbook of LHC Higgs Cross Sections: 3. Higgs Properties," arXiv:1307.1347

[5] S. Dittmaier *et al.* [LHC Higgs Cross Section Working Group Collaboration], *"Handbook of LHC Higgs Cross Sections: 1. Inclusive Observables,"* arXiv:1101.0593

[6] Michael E. Peskin, Dan V. Schroeder, *An Introduction To Quantum Field Theory*, Westview Press, 1995.

[7] S. L. Glashow, Partial Symmetries of Weak Interactions, Nuc. Phys. 22 (1961) 579.

[8] A. Salam, Weak and Electromagnetic Interactions, Conf. Proc. C 680519 (1968) 367. Originally printed in Svartholm: Elementary Particle Theory, proceedings of the Nobel Symposium held 1968 at Lerum, Sweden.

[9] S. Weinberg, A Model of Leptons, Phys. Rev. Lett. 19 (1967) 1264.

[10] H. Fritsch, M. Gell-Mann, and H. Leutwyler, Advantages of the Color Octet Gluon Picture, Phys. Lett. B 47 (1973) 365.

[11] F. Englert and R. Brout, *Broken Symmetry and the Mass of Gauge Vector Mesons*, Phys. Rev. Lett. **13** (1964) 321.

[12] P. W. Higgs, *Broken symmetries, massless particles and gauge fields*, Phys. Lett. **12** (1964) 132.

[13] P. W. Higgs, *Broken Symmetries and the Masses of Gauge Bosons*, Phys. Rev. Lett. **13** (1964) 508.

[14] P. W. Higgs, *Spontaneous Symmetry Breakdown without Massless Bosons*, Phys. Rev. **145** (1966) 1156.

[15] T. W. B. Kibble, Symmetry Breaking in NonAbelian Gauge Theories, Phys. Rev. 155 (1967) 1554.

[16] The ATLAS Collaboration, *Observation of a new particle in the search for the Standard Model Higgs boson with the ATLAS detector at the LHC*, Physics Letters B **716** (2012) 1–29.

[17] The CMS Collatoration, *Observation of a new boson at a mass of 125 GeV with the CMS experiment at the LHC*, Physics Letters B **716** (2012) 30–61.

[18] W. Hollik, *"Electroweak theory,"* hep-ph/9602380.

[19] The Review of Particle Physics, J. Beringer et al. (Particle Data Group), Phys. Rev. D86, 010001 (2012) and 2013 partial update for the 2014 edition.

[20] The ALEPH, CDF, D0, DELPHI, L3, OPAL and SLD Collaborations, the LEP Electroweak Working Group, Tevatron Working Group and SLD Electroweak and Heavy Flavour Working Groups, *Precision Electroweak Measurements and Constraints on the Standard Model*, arXiv:1012.2367. Updated for 2012 winter conferences, March 2012.

[21] The Gfitter Group, M. Baak, et al., Updated Status of the Global Electroweak Fit And constraints on New Physics, Eur. Phys. J. C 72 (2012) 2003. Updated for 2012 winter conferences, March 2012, http://gfitter.desy.de.

[22] G.W. Bennett et al., Phys. Rev. Lett. 89, 101804 (2002); Erratum ibid. Phys. Rev. Lett. 89, 129903 (2002); G.W. Bennett et al., Phys. Rev. Lett. 92, 161802 (2004); G.W. Bennett et al., Phys. Rev. D73, 072003 (2006).

[23] B. Bhattacherjee, S. S. Biswal and D. Ghosh, *Top quark forward-backward asymmetry at Tevatron and its implications at the LHC*, Phys. Rev. D **83** (2011) 091501 [arXiv:1102.0545 [hep-ph]].

[24] M. Veltman, Acta. Phys. Pol. B8 (1977) 475.

[25] S. Weinberg, Gauge Hierarchies, Phys. Lett. B 82 (1979) 387.

[26] M. Veltman, The InfraredUltraviolet Connection, Acta Phys. Polon. B 12 (1981) 437.

[27] C. Smith and G. Ross, The Real Gauge Hierarchy Problem, Phys. Lett. B 105 (1981) 38.

[28] F. Zwicky, Spectral Displacement of Extra Galactic Nebulae, Helv. Phys. Acta 6 (1933) 110.

[29] E. W. Kolb and M. S. Turner, The Early Universe, Front. Phys. 69 (1990) 1.

[30] The WMAP Collaboration, D. N. Spergel et al., First Year Wilkinson Microwave Anisotropy Probe (wmap) Observations: Determination of Cosmological Parameters, Astrophys. J. Suppl. 148 (2003) 175.

[31] H. M. Georgi and S. L. Glashow, Unity of All ElementaryParticle Forces, Phys. Rev. Lett. 32 (1974) 438.

[32] J. C. Pati and A. Salam, Lepton Number as the Fourth Color, Phys. Rev. D 10 (1974) 275.

[33] P. Fayet, Phys. Lett. B 64, 159 (1976).

[34] P. Fayet, Phys. Lett. B 69, 489 (1977), Phys. Lett. B 84, 416 (1979).

[35] G.R. Farrar and P. Fayet, Phys. Lett. B 76, 575 (1978).

[36] S. Martin, in Perspectives on Supersymmetry, Ed. G.L. Kane, World Scientific, Singa- pore, 1998, hep-ph/9709356.

[37] For reviews on the MSSM, see: P. Fayet and S. Ferrara, Phys. Rep. 32 (1977) 249; H.P. Nilles, Phys. Rep. 110 (1984) 1; R. Barbieri, Riv. Nuovo Cim. 11N4 (1988) 1; R. Arnowitt and Pran Nath, Report CTP-TAMU-52-93; J. Bagger, Lectures at TASI-95, hep-ph/9604232.

[38] H. E. Haber and G. Kane, Phys. Rep. 117 (1985) 75.

[39] M. Drees and S. Martin, CLTP Report (1995) and hep-ph/9504324.

[40] D.J.H. Chung, L.L. Everett, G.L. Kane, S.F. King, J. Lykken and L.T. Wang, Phys. Rept. 407 (2005) 1.

[41] M. Drees, R.M. Godbole and P. Roy, Theory and Phenomenology of Sparticles, World Scientific, Spring 2004.

[42] L. Girardello and M.T. Grisaru, Nucl. Phys. B194 (1982) 65.

[43] Y. Okada, M. Yamaguchi and T. Yanagida, Prog. Theor. Phys. 85 (1991) 1; ibid. Phys. Lett. B262 (1991) 54; J.R. Ellis, G. Ridolfi and F. Zwirner, Phys. Lett. B257 (1991) 83; ibid. Phys. Lett. B262 (1991) 477; H.E. Haber and R. Hempfling, Phys. Rev. Lett. 66 (1991) 1815.

[44] A. Djouadi and S. RosiersLees (conv.) et al., Summary Report of the MSSM Working Group for the GDRSupersym trie, hep-ph/9901246.

[45] K. Inoue, A. Komatsu and S. Takeshita, Prog. Theor. Phys 68 (1982) 927; (E) ibid. 70 (1983) 330.

[46] E. Witten, Nucl. Phys. B188 (1981) 513; ibid Nucl. Phys. B202 (1982) 253; N. Sakai, Z. Phys. C11 (1981) 153; S. Dimopoulos and H. Georgi, Nucl. Phys. B193 (1981) 150; R.K. Kaul and P. Majumdar, Nucl. Phys. B199 (1982) 36.

[47] J.F. Donoghue and L.F. Li, Phys. Rev. 19 (1979) 945.

[48] J.F. Gunion and H.E. Haber, Nucl. Phys. B278 (1986) 449.

[49] J.F. Gunion and H.E. Haber, Nucl. Phys. B272 (1986) 1; (E) hep-ph/9301205.

[50] M. Frank et al., The Higgs Boson Masses and Mixings of the Complex MSSM in the FeynmanDiagrammatic Approach, JHEP 0702 (2007) 47.

[51] M. Carena, S. Heinemeyer, C. E. M. Wagner, and G. Weiglein, *Suggestions for benchmark scenarios for MSSM Higgs boson searches at hadron colliders*, Eur. Phys. J. **C26** (2003) 601–607, `hep-ph/0202167`.

[52] S. Heinemeyer, O. Stal, and G. Weiglein, *Interpreting the LHC Higgs Search Results in the MSSM*, Phys. Lett. B 710 (2012) 201206, arXiv:1112.3026.

[53] The ATLAS Collaboration , *Constraints on New Phenomena via Higgs Boson Coupling Measurements with the ATLAS Detector.* ATLAS-CONF-2014-010.

[54] L. Maiani, A. Polosa, and V. Riquer, Bounds to the Higgs Sector Masses in Minimal Supersymmetry from LHC Data, arXiv:1305.2172.

[55] A. Djouadi, L. Maiani, G. Moreau, A. Polosa, J. Quevillon, et al., The post-Higgs MSSM scenario: Habemus MSSM?, arXiv:1307.5205.

[56] L. Evans and P. Bryant, *LHC Machine*, JINST **3** (2008) S08001.

[57] The ATLAS Collaboration, G. Aad et al., *The ATLAS Experiment at the CERN Large Hadron Collider*, JINST **3** (2008) S08003.

[58] J. Haffner, *The CERN accelerator complex*, OPEN-PHO-ACCEL-2013-056.

[59] CMS Collaboration, CMS technical proposal, CERN-LHCC-94-38.

[60] LHCb Collaboration, LHCb technical proposal, CERN-LHCC-98-004.

[61] ALICE Collaboration, ALICE: Technical proposal for a large ion collider experiment at the CERN LHC, CERN-LHCC-95-71, CERN, 1995,

[62] G. S. Guralnik, C.R. Hagen and T. W. B. Kibble Phys.Rev.Lett. **13** (1964) 585.

[63] The ATLAS Collaboration, *Luminosity Determination in pp Collisions at* $\sqrt{s} = 7$ *TeV using the ATLAS Detector in 2011*, ATLAS-CONF-2011-116.

[64] ALEPH, DELPHI, L3 and OPAL Collaboration, *Search for neutral MSSM Higgs bosons at LEP*, Eur. Phys. J. **C47** (2006) 547.

[65] *Combined CDF and D0 upper limits on MSSM Higgs boson production in tau-tau final states with up to 2.2* fb^{-1} *of data*, `arXiv:1003.3363 [hep-ex]`.

[66] The CMS Collaboration, S. Chatrchyan et al., `arXiv:1104.1619 [hep-ex] [hep-ex]`.

[67] The ATLAS Collaboration , *Search for the neutral Higgs bosons of the Minimal Supersymmetric Standard Model in pp collisions at* $\sqrt{s} = 7$ *TeV with the ATLAS detector*, `arXiv:1211.6956 [hep-ex]`.

[68] S. Heinemeyer, O. Stål and G. Weiglein, *Interpreting the LHC Higgs search results in the MSSM*, Phys.Lett. **B710** (2012) 201–206, `arXiv:1112.3026 [hep-ph]`.

[69] A. Arbey, M. Battaglia, A. Djouadi and F. Mahmoudi, *The Higgs sector of the phenomenological MSSM in the light of the Higgs boson discovery*, JHEP **1209** (2012) 107, `arXiv:1207.1348 [hep-ph]`.

[70] M. L. Mangano et al., *ALPGEN, a generator for hard multiparton processes in hadronic collisions*, JHEP **07** (2003) 001.

[71] J. Alwall et al., *Comparative study of various algorithms for the merging of parton showers and matrix elements in hadronic collisions*, Eur. Phys. J. **C53** (2008) 473, `arXiv:0706.2569`.

[72] S. Frixione and B. R. Webber, *Matching NLO QCD computations and parton shower simulations*, JHEP **06** (2002) 029, `hep-ph/0204244`.

[73] B. P. Kersevan and E. Richter-Was, *The Monte Carlo Event Generator AcerMC 2.0 with Interfaces to PYTHIA 6.2 and HERWIG 6.5*, `arXiv:0405247v1 [hep-ph]`.

[74] G. Corcella et al., *HERWIG 6: an event generator for hadron emission reactions with interfering gluons (including supersymmetric processes)*, JHEP **01** (2001) 010.

[75] J. M. Butterworth, J. R. Forshaw, and M. H. Seymour, *Multiparton Interactions in Photoproduction at HERA*, Z. Phys. **C72** (1996) 637.

[76] T. Binoth, M. Ciccolini, N. Kauer, and M. Kramer, *Gluon-induced W-boson pair production at the LHC*, JHEP **12** (2006) 046.

[77] A. S. et al., *Higgs boson production in gluon fusion*, JHEP **02** (2009) 029.

[78] T. Gleisberg et al., *Event generation with SHERPA 1.1*, JHEP **02** (2009) 007.

[79] J. Pumplin, D. R. Stump, J. Huston, H. L. Lai, P. M. Nadolsky and W. K. Tung, "New generation of parton distributions with uncertainties from global QCD analysis," JHEP **0207** (2002) 012 [hep-ph/0201195].

[80] H. -L. Lai, M. Guzzi, J. Huston, Z. Li, P. M. Nadolsky, J. Pumplin and C. -P. Yuan, "New parton distributions for collider physics," Phys. Rev. D **82** (2010) 074024 [arXiv:1007.2241 [hep-ph]].

[81] The ATLAS Collaboration, *ATLAS Monte Carlo Tunes for MC09*, ATL-PHYS-PUB-2010-002.

[82] S. Jadach, J. H. Kuhn and Z. Was, *TAUOLA - a library of Monte Carlo programs to simulate decays of polarized τ leptons*, Comput. Phys. Commun. **64** (1990) 275.

[83] E. Barberio, B. V. Eijk and Z. Was, *Photos - a universal Monte Carlo for QED radiative corrections in decays*, Comput. Phys. Commun. **66** (1991) 115.

[84] The GEANT4 Collaboration, S. Agostinelli et al., *GEANT4 - a simulation toolkit*, Nucl. Instrum. Meth. **A506** (2003) 250.

[85] The ATLAS Collaboration, G. Aad et al., *The ATLAS Simulation Infrastructure*, ATLAS-SOFT-2010-01-004, submitted to Eur. Phys. J. C., `arXiv:1005.4568`.

[86] The ATLAS Collaboration, *Estimation of $Z/\gamma^* \to \tau\tau$ Background in VBF $H \to \tau\tau$ Searches from $Z \to \mu\mu$ Data using an Embedding Technique*, ATL-PHYS-INT-2009-109.

[87] The ATLAS Collaboration, *Search for the Standard Model Higgs boson in the $H \to \tau\tau$ decay mode with $4.7 fb1$ of ATLAS detector*, Tech. Rep. ATLAS-CONF-2012-014, CERN, Geneva, Mar, 2012.

[88] The ATLAS Collaboration, *Search for the Standard Model Higgs boson $H \to \tau\tau$ decays with the ATLAS detector*, ATL-COM-PHYS-2013-722.

[89] T. S. et al., Z *physics at LEP 1*, CERN 89-08 **3** (1989) 143.

[90] The ATLAS Collaboration, Inner Detector: Technical Design Report, CERN/LHCC/97-016/017 (1997).

[91] The ATLAS Collaboration, G. Aad et al., The ATLAS Experiment at the CERN Large Hardon Collider, 2008 JINST 3 S08003.

[92] A. Bazan, T. Bouedo, P. Ghez, M. Marino and C. Tull, "The Athena data dictionary and description language," eConf C **0303241** (2003) MOJT010 [cs/0305049 [cs-se]].

[93] The ATLAS Collaboration, *Expected Performance of the ATLAS Experiment - Detector, Trigger and Physics*, CERN-OPEN-2008-020, `arXiv:0901.0512`.

[94] T. Cornelissen et al., Concepts, Design and Implementation of the ATLAS New Tracking, ATLAS Note ATL-SOFT-PUB-2007-007 (2007).

[95] Kalman, R. E. (1960). *"A New Approach to Linear Filtering and Prediction Problems"*. Journal of Basic Engineering 82 (1): 3545. doi:10.1115/1.3662552

[96] The ATLAS Collaboration, Performance of primary vertex reconstruction in proton-proton collisions at $s = sqrt(7)$ TeV in the ATLAS experiment. ATLAS-CONF-2010-069.

[97] R. Fruhwirth, W. Waltenberger, P. Vanlaer, *Adaptive vertex fitting*, J. Phys. G34 (2007).

[98] The ATLAS Collaboration, *Characterization of Interaction-Point Beam Parameters Using the pp Event-Vertex Distribution Reconstructed in the ATLAS Detector at the LHC*, ATL-CONF-2010-027.

[99] The ATLAS collaboration, *Expected electron performance in the ATLAS experiment*, ATL-PHYS-PUB-2011-006

[100] The ATLAS Collaboration, *Electron reconstruction and identification efficiency measurements with the ATLAS detector using the 2011 LHC proton-proton collision data*, CERN-PH-EP-2014-040, arXiv:1404.2240

[101] The ATLAS Collaboration, G. Aad et al., *Electron performance measurements with the ATLAS detector using the 2010 LHC proton-proton collision data*, Eur.Phys.J. C72 (2012) 1909.

[102] S. Hassini, et al., *A muon identification and combined reconstruction procedure for the ATLAS detector at the LHC using the (MUONBOY, STACO, MuTag) reconstruction packages*, NIM A572 (2007) 7779.

[103] The ATLAS Collaboration, G. Aad et al., *Preliminary results on the muon reconstruction efficiency, momentum resolution, and momentum scale in ATLAS 2012 pp collision data*, ATLAS-CONF-2013-088, CERN, 2013,

[104] M. Cacciari, G. P. Salam, and G. Soyez, *FastJet user manual*, Eur.Phys.J. C72 (2012) 1896.

[105] W. Lampl et al., *Calorimeter Clustering Algorithms : Description and Performance*, ATL-LARG-PUB-2008-002.

[106] M. Cacciari, G. P. Salam, and G. Soyez, *The anti-kt jet clustering algorithm*, JHEP 04 (2008) 63.

[107] E. Abat, J. Abdallah, T. Addy, P. Adragna, et al., *Combined performance studies for electrons at the 2004 ATLAS combined test-beam*, JINST 5 (2010) P11006.

[108] ATLAS Collaboration, *Jet energy measurement with the ATLAS detector in proton-proton collisions at* $\sqrt{s} = 7$ *TeV*, Submitted to EPJ (2011) , arXiv:1112.6426

[109] The ATLAS Collaboration, *Pile-up corrections for jets from proton-proton collisions at ATLAS in 2011*, ATLAS-CONF-2012-064, July, 2012.

[110] M. Cacciari and G. P. Salam, *Pileup subtraction using jet areas*, Phys.Lett. B659 (2008) 119.

[111] The ATLAS Collaboration, G. Aad et al., *Jet energy resolution in proton-proton collisions at* $\sqrt{s} = 7$ *TeV recorded in 2010 with the ATLAS detector*, Eur.Phys.J. C73 (2013) 2306

[112] The ATLAS collaboration, *Jet energy scale and its systematic uncertainty in proton-proton collisions at* $\sqrt{s} = 7$ *TeV with ATLAS 2011 data*, ATLAS-CONF-2013-004

[113] The ATLAS Collaboration, *Data-Quality Requirements and Event Cleaning for Jets and Missing Transverse Energy Reconstruction with the ATLAS Detector in Proton-Proton Collisions at a Center-of-Mass Energy of* $\sqrt{s} = 7$ *TeV*, ATLAS-CONF-2010-038.

[114] G. Piacquadio, C. Weiser, *A new inclusive secondary vertex algorithm for b-jet tagging in ATLAS*, JPCS 119 (2008) 032032

[115] The ATLAS Collaboration, G. Aad et al., *Commissioning of the ATLAS high-performance b-tagging algorithms in the 7 TeV collision data, ATLAS-CONF-2011-102*, CERN, 2011, ATLAS-CONF-2011-102.

[116] The ATLAS Collaboration, *Measuring the b-tag efficiency in a ttbar sample with 4.7* fb^{-1} *of data from the ATLAS detector* ATLAS-CONF-2012-097.

[117] The ATLAS Collaboration, *Calibration of b-tagging using dileptonic top pair events in a combinatorial likelihood approach with the ATLAS experiment* ATLAS-CONF-2014-004.

[118] The ATLAS Collaboration, *Reconstruction and Calibration of Missing Transverse Energy and Performance in Z and W events in ATLAS Proton-Proton Collisions at* $\sqrt{s}$*=7 TeV*, ATLAS-CONF-2011-080.

[119] ATLAS Collaboration, G. Aad et al., Performance of missing transverse momentum reconstruction in proton-proton collisions at 7 TeV with ATLAS, Eur.Phys.J. C72 (2012) 1844.

[120] TheATLAS Collaboration, *Performance of the Reconstruction and Identification of Hadronic tau Decays in ATLAS with 2011 Data*, ATLAS-CONF-2012-142.

[121] The ATLAS Collaboration, G. Aad et al., *Performance of the ATLAS trigger system in 2010*, Eur.Phys.J. C72 (2012) 1849.

[122] The ATLAS Collaboration, G. Aad et al., *Performance of the ATLAS muon trigger in 2011*, ATLAS-CONF-2012-099, CERN, 2012.

[123] The ATLAS Collaboration, G. Aad et al., *Performance of the ATLAS electron and photon trigger in p-p collisions at* $\sqrt{s} = 7$ *TeV in 2011*, ATLAS-CONF-2012-048, CERN, 2012.

[124] M. Dobbs and J.B. Hansen, *The HepMC C++ Monte Carlo Event Record for High Energy Physics*, Computer Physics Communications, ATL-SOFT-2000-001.

[125] The ATLAS Collaboration, *Evidence for the spin-0 nature of the Higgs boson using ATLAS data* , Phys. Lett. B 726 (2013), pp. 120-144.

[126] The ATLAS Collaboration, *Measurements of Higgs boson production and couplings in diboson final states with the ATLAS detector at the LHC*, Phys. Lett. B 726 (2013), pp. 88-119.

[127] The CMS Collaboration, *"Evidence for the direct decay of the 125 GeV Higgs boson to fermions,"* arXiv:1401.6527 [hep-ex].

[128] The CMS Collaboration, *Higgs boson width from on- vs. off-shell production and decay to Z-boson pairs* , arXiv:1405.3455.

[129] A. Elagin, P. Murat, A. Pranko, and A. Safonov, *A New Mass Reconstruction Technique for Resonances Decaying to di-tau*, arXiv:1012.4686 [hep-ex]. * Temporary entry *.

[130] T. A. Collaboration, *Search for neutral MSSM Higgs bosons decaying to $\tau\tau$ pairs in proton-proton collisions at with the ATLAS detector*, Physics Letters B **705** (2011) no. 3, 174 – 192.

[131] The ATLAS Collaboration, *Data-driven estimation of the background to charged Higgs boson searches using hadronically-decaying tau final states in ATLAS,* ATLAS-CONF-2011-051.

[132] The ATLAS Collaboration, *Measurement of the $Z \to \tau\tau$ cross section with the ATLAS detector*, Phys. Rev. D **84** (2011) 112006.

[133] T. A. Collaboration, *Search for the neutral Higgs bosons of the Minimal Supersymmetric Standard Model in pp collisions at $\sqrt{s} = 7$ TeV with the ATLAS detector*, JHEP , arXiv:1211.6956.

[134] Atlas statistics forum, *ABCD method in searches*, link

[135] The ATLAS Collaboration, *Search for Neutral MSSM Higgs Bosons H to $\tau\tau$ to $l\tau_h$ with the ATLAS Detector in 7 TeV Collisions*, ATL-COM-PHYS-2012-094.

[136] The ATLAS Collaboration, *Search for neutral Higgs Bosons in the decay mode $H \to \tau\tau \to ll{+}4\nu$ in proton proton collision at $\sqrt{7}$ TeV with the ATLAS Detector*, ATL-COM-PHYS-2011-758.

[137] The Atlas Collaboration, *Measurement of the ttbar production cross-section in pp collisions at $\sqrt{s} = 8$ TeV using e-mu events with b-tagged jets* . ATLAS-CONF-2013-097.

[138] T. Sjostrand, S. Mrenna and P. Skands, *PYTHIA 6.4 physics and manual*, JHEP **05** (2006) 026.

[139] A. B. et al., *Rivet user manual*, arXiv:1003.0694 [hep-ph].

[140] The ATLAS and CMS Collaborations, *Procedure for the LHC Higgs boson search combination in summer 2011*, ATL-PHYS-PUB-2011-011, ATL-COM-PHYS-2011-818, CMS-NOTE-2011-005.

[141] W. Verkerke and D. P. Kirkby, *The Roofit Toolkit for Data Modeling*, eConf C0303241 (2003) MOLT007, arXiv:physics/0306116

[142] K. S. Cranmer et al., *The Roostats Project*, PoS ACAT2010 (2010) 57.

[143] K. Cranmer, G. Lewis, L. Moneta, A. Shibata, and W. Verkerke, *Histfactory: A Tool for Creating Statistical Models for use with Roofit and Roostats*, CERNOPEN2012016 (2012)

[144] E. G. G. Cowan, K. Cranmer and O. Vitells, *Asymptotic formulae for likelihood-based tests of new physics*, `arXiv:1007.1727 [hep-ex]`.

[145] A. L. Read. *Presentation of search results: the CLs technique*. J. Phys. G: Nucl. Part. Phys., 28, 2002.

[146] A. L. Read. *Modified frequentist analysis of search results (the CLs method)*. In Proceedings of the First Workshop on Confidence Limits, CERN, Geneva, Switzerland, 2000.

[147] LHC Higgs Cross Section Working Group, S. Dittmaier, C. Mariotti, G. Passarino, R. Tanaka (Eds.), et al., *Handbook of LHC Higgs Cross Sections: 1. Inclusive Observables*, `arXiv:1101.0593 [hep-ph]`.

[148] LHC Higgs Cross Section Working Group, S. Dittmaier, C. Mariotti, G. Passarino, and R. Tanaka (Eds.), *Handbook of LHC Higgs Cross Sections: 2. Differential Distributions*, CERN-2012-002 (CERN, Geneva, 2012) , `arXiv:1201.3084 [hep-ph]`.

[149] ATLAS collaboration *Performance of the ATLAS Silicon Pattern Recognition Algorithm in Data and Simulation at* $\sqrt{s} = 7$ *TeV*, ATLAS-CONF-2010-072

[150] The ATLAS Collaboration, *A measurement of the material in the ATLAS inner detector using secondary hadronic interactions*, arXiv:1110.6191, JINST 7 (2012) P01013

[151] The ATLAS Collaboration, *Validation of the ATLAS jet energy scale uncertainties using tracks in proton-proton collision* $\sqrt{s} = 7$ *TeV*, ATLAS-CONF-2011-067

[152] The ATLAS Collaboration, *Track Reconstruction Efficiency in* $\sqrt{s} = 7$ *TeV Data for Tracks with* $p_T > 100$ *MeV* , ATL-PHYS-INT-2010-112

[153] D. de Florian, G. Ferrera, M. Grazzini and D. Tommasini, *Transverse-momentum resummation: Higgs boson production at the Tevatron and the LHC*, JHEP **1111** (2011) , `arXiv:1109.2109 [hep-ph]`.

[154] Statistical twiki, NuissanceCheck. https://twiki.cern.ch/twiki/bin/view/AtlasProtected/Nuisa